

Supporting information

Electrostatic Directed Assembly of Colloidal Microparticles Assisted by Convective Flow

*Lauryanne Teulon¹, Yannick Hallez², Simon Raffy¹, François Guerin¹, Etienne Palleau¹ and
Laurence Ressier^{1,*}*

¹LPCNO, Université de Toulouse, CNRS, INSA, UPS, 135 Avenue de Rangueil, 31077
Toulouse, France

²Laboratoire de Génie Chimique, Université de Toulouse, CNRS, INPT, UPS, Toulouse,
France

* Author to whom correspondence should be addressed: laurence.ressier@insa-toulouse.fr /
+33(0)5.61.55.96.72

Materials

Colloidal dispersions of fluorescent carboxylate latex particles with five different diameters (100 nm, 500 nm, 1 μm , 4.3 μm and 10 μm) were purchased from PolyScience[®] (Fluoresbrite[®] YG Carboxylate Microspheres, $\lambda_{em} \approx 486$ nm). These negatively charged particles were chosen as model ones for this study because they exist in a same size assortment and their fluorescence helps their characterization by optical microscopy. Prior to use, all solutions were centrifuged at 15000 rpm during 30min in water to remove excess ligands. Isopropanol (IPA, 99.5%) was then used to dilute particle dispersions for all experiments.

Electrical microcontact printing (e- μ CP)

The first step of the nanoxerography protocol was performed by electrical microcontact printing method (e- μ CP) on 100 nm PolyMethylMethAcrylate thin films spin-coated on highly doped silicon wafers. A magnetic and electrically conductive PolyDiMethySiloxane stamp featuring patterns of desired geometries was used. Following a previously described protocol¹ based on a modified Innostamp 40 equipment, a magnetic pressure was applied owing to a matrix of magnets carefully positioned under the substrate. It allowed to ensure a homogeneous and reproducible contact between the PMMA thin film and the patterned stamp even on large surfaces up to a 4 inch wafer.² A DC voltage of 40V was applied between the conductive PDMS stamp and the substrate during 45s. It resulted in the creation of multiple positively charged snowflakes patterns with a 250 μm width. The choice of such micrometer wide patterns facilitates the in-situ optical observations and characterization of large latex particles assemblies, while showing complex details on their branches.

1 μm latex particles assembly by conventional nanoxerography using immersion development

Conventional nanoxerography protocol including a manual immersion of a charged sample in a colloidal bath followed by manual withdrawal was used to assemble negatively charged 1 μm latex particles. A fixed colloidal dispersion concentration of $\rho_0 = 6.825 \times 10^8 \text{ mL}^{-1}$ was used while varying t_{sc} between 30s and 5min.

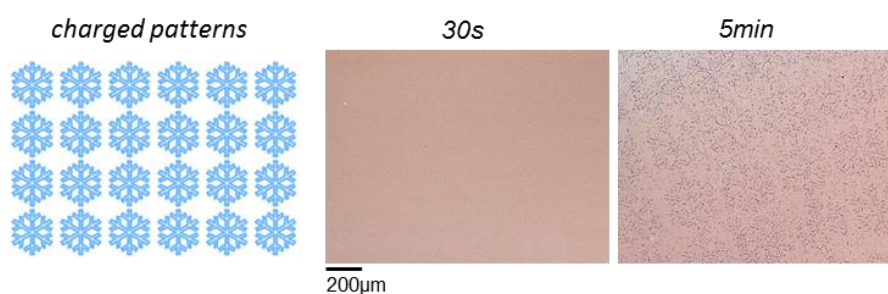


Figure S1. Image of the expected charged patterns given for sake of clarity (left). Optical microscopy image of 1 μm particle assemblies made with nanoxerography using a static contact time of either 30s (middle) or 5min (right).

No particle assembly was observed for $t_{sc} = 30\text{s}$ while some particle assembly, with poor density and selectivity, was obtained for $t_{sc} = 300\text{s}$ and a slow manual withdrawal of the substrate. These experiments also reveal that the way the solvent evaporates during t_{dc} strongly affects the particle assembly. A natural (non-controlled) evaporation of the solvent indeed leads to a seemingly random dewetting of the substrate and to the creation of several dispersion droplets. Evaporation of the latter generates particle aggregates at locations independent of the presence of charged patterns.

Convective nanoxerography set up

A homemade CSA deposition system was used to drag a drop of colloidal dispersion using a glass blade inclined at an angle of 20° at 200-300 μm above the horizontal substrate fixed to a temperature-regulated copper plate (see **Scheme 1** of the paper). Temperature regulation was controlled from 17°C to 25°C . A 10-15 μL particle dispersion drop was injected between the blade and the substrate. The meniscus formed by the colloidal dispersion over the substrate was put in translational motion by dragging the stage under the substrate at dragging speeds ranging from 5 to 100 $\mu\text{m}\cdot\text{s}^{-1}$. All experiments were performed in ambient air, at room

temperature (20°C), and a relative humidity RH 40%. The setup was mounted under an optical microscope to allow real-time observations.

A syringe pump system was used to balance the solvent evaporation during the static contact time analysis. First, the 10-15 μL drop of the particle dispersion was deposited between the glass blade and the charged substrate. Then the syringe pump system was used to have a continuous supply of solvent (IPA). The whole system was set to locate the needle below the glass slide at the back of the dispersion drop. An IPA flow rate of 1.11 $\mu\text{L}/\text{min}$ was fixed thanks to empirical determination of the pure solvent evaporation rate. The pumping system was turned on during the whole static contact period of time, the needle was removed at the end of it and the stage was translated to go on the convective flow development with parameters depending on the final aim.

Matlab image analysis program

To determine the particle density on a snowflake pattern while assembling 1 μm latex particles, a homemade Matlab[®] program was used to analyze fluorescent optical microscopy images. From these optical images, four particle based snowflake patterns were observed by sample to evaluate the reproducibility of the process.

The pictures used in the analysis program were taken by a microscope under fluorescent conditions equipped with a 20x (while observing particles on patterns) and 50x (while observing particles out of patterns) magnification. To start the analysis, the blue matrix of the RGB 8 bits microscopic picture (0 to 255) is extracted. To select the particles on the snowflake pattern, the blue image is multiplied by a logical image L1 of the snowflake pattern: the value 1 if on, and 0 if out of patterns: everything out of the pattern is consequently considered to be zero. A logical condition is applied to the image with a threshold T1 fixed at a level corresponding to half the maximum level of the image in order to separate particles and particle clusters from the background. A new small matrix is created for each separated object (single particles or particle clusters). All these small matrices are then multiplied by the corresponding part of the blue matrix (**Figures S2.a-b**).

For each small matrix, an iteration is used from the level corresponding to half of the maximum level of the blue matrix up to the maximum one. Each iteration value leads to a threshold T2 to get various logical images. The average coordinates x and y are calculated from all 1 values of

all logical images. With those data, statistical centers or centroids of the objects/particles are obtained (see red cross on Figure S2a&b). A profile is created with the blue matrix levels as a function of the length of each pixel to these centroids (**Figures S2.c-d**).

After the analysis treatment, a single particle has a near-Gaussian profile (see **Figure S2.c**) while other objects (two particles or more) have hysteresis like profiles (see **Figure S2.d**). By derivating such profiles, single particles from multiple ones are separated.

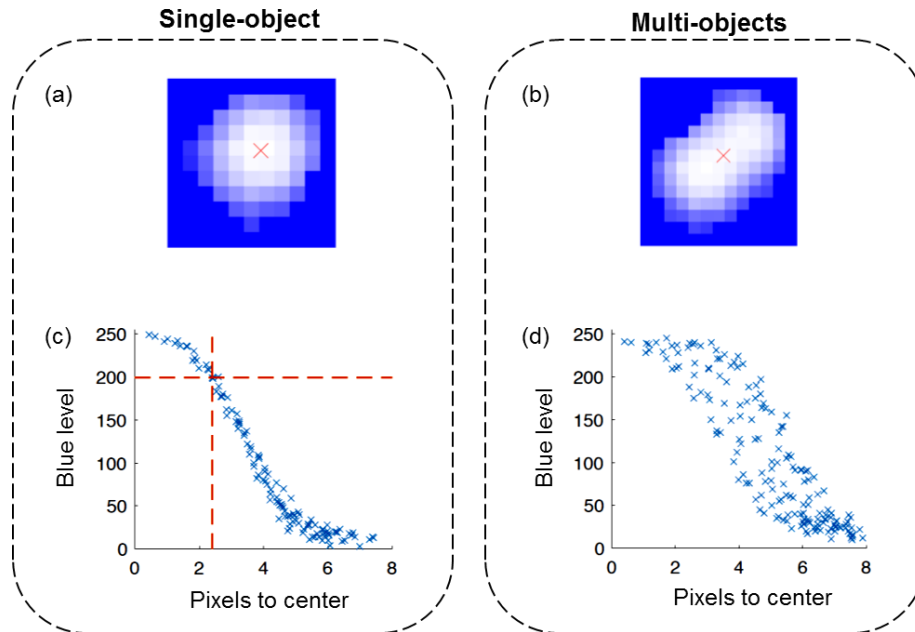


Figure S2. Image analysis for (a,c) single object (b,d) multi-objects. (a,b) Numerical images created for the analysis. The red crosses are the positions of the calculated centers. The solid blue is the threshold (where logical images = 0). The interne color variations are the corresponding part of the blue matrix. (c,d) Profiles of the particles: blue level as a function of the length of each pixel to the center.

The comparison of the real radius of one particle (converted in pixels) with a single particle profile gives a specific blue level, further used as a threshold T3. This comparison is done for each single particle detected on the full image.

The average value of all T3 thresholds gives a threshold T4 applied on each object (single or multiple particles) to shape them to their physical dimensions converted to specific pixel areas. These pixel areas are divided by the real physical cross-section of a particle (converted in pixels²) to get a normalized number of particles for each object (*Nb*).

Due to the fluorescent overlapping when considering particle clusters, the image treatment detailed above results in the addition of extra pixels (an extra artefact surface S) at the interfaces between particles that virtually increase the number of pixels in the case of complex objects

(two or more particle based clusters). To find the correct number of particles (Nb_{cor}), a logistic map is applied to all Nb (equation 1).

$$Nb_{cor} = Nb - 2 * \alpha * (Nb - 1) \quad (1)$$

Where α is the corrective factor (between 0 and 0.2) corresponding to S . α is adjusted to get the best fit with the integer number of particles by objects (**Figure S3**).

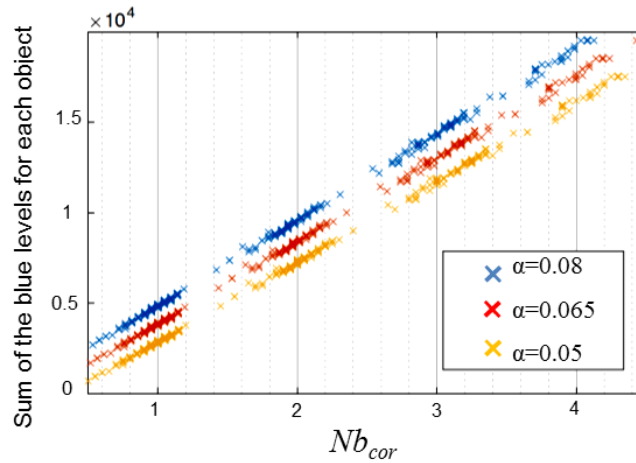


Figure S3. Sum of the blue levels of each object as function of Nb_{cor} in the case of an assembly of $1 \mu\text{m}$ particles (dragging speed $8\mu\text{m}\cdot\text{s}^{-1}$, $t_{ic} = 275\text{s}$, concentration = $3\rho_0/2$). Blue and yellow set of points have respectively an ordinate offset $+10^3$ and -10^3 for sake of clarity.

The number of particles on each snowflake pattern is given by the sum ΣNb_{cor} . The Nb_{cor} for $\alpha = 0,065$ gives the best fit for the objects from 1 to 4 particles (**Figure S3**).

It is worth noting that, since α is manually defined, it induces some errors that have to be taken into account. These errors calculated for all images, vary from 1 to 9%.

The sum of all pixels of a logical image L1 gives a pattern area with pixel^2 as unit. To get the final particle density, the number of particles is divided by the surface of the corresponding snowflake pattern. With the magnitude of the microscope, the unit is converted from $\text{particle}/\text{pixel}^2$ to $\text{particle}/\text{mm}^2$.

Determination of the electrostatic boundary condition on 1 μ m latex particles in isopropanol

The electrophoretic mobility of 1 μ m latex particles in isopropanol was measured with a Zeta Potential Particle Analyzer (Beckman Coulter) for a wide range of particle volume fraction $10^{-5} < \phi < 10^{-2}$ (**Figure S4**). Data were an average of 5 measurements with 30s acquisition times. The samples were allowed to equilibrate thermally at the desired temperature for 5min before the measurements. Electrophoretic mobility was calculated using the Laser Doppler Method. In this system, the mobility decreases with volume fraction even in relatively dilute conditions due to the presence of long-range interactions. This behavior is dependent on the balance between hydrodynamic and electrostatic forces, the latter depending on the electrostatic boundary condition (BC) on the surface of particles. These BC can thus be deduced from the fitting of experimental data with an adequate model. Here we used an expression developed by Ohshima with a cell model.³ This expression, valid in the context of the linearized Debye Hückel theory for electrostatics, reads

$$\mu = \frac{2\epsilon\zeta}{3\eta} \int_a^b H(r) \left(1 + \frac{a^3}{2r^3}\right) dr + \frac{2\epsilon(\kappa a)^2}{9\eta(1-\phi)} \psi^{(0)}(b) \left(1 + \frac{a^3}{2b^3}\right) \left(1 + \frac{b^3}{a^3} - \frac{9b^2}{5a^2} - \frac{a^3}{5b^3}\right),$$

where

$$H(r) = -\frac{(\kappa a)^2}{6\zeta(1-\phi)} \left[1 - \frac{3r^2}{a^2} + \frac{2r^3}{a^3} - \frac{a^3}{b^3} \left(\frac{2}{5} - \frac{r^3}{a^3} + \frac{3r^5}{5a^5} \right) \right] \frac{d\psi^0}{dr} \quad (2)$$

and a is the particle radius, $b = a\phi^{-\frac{1}{3}}$ is the radius of the cell, ϵ is the solvent dielectric constant and η its dynamic viscosity, ζ is the particle effective surface potential, κ^{-1} is the effective screening length, and $\psi^{(0)}$ is the (unscaled) electrostatic potential field in the cell model. This expression has then been fitted to the experimental mobility data by adjusting κ and ζ . The consistence between theoretical and experimental data for constant values of these parameters ($\kappa a = 0.05$ and $\zeta = 0.086$ V) indicate that a constant effective surface potential is pertinent for the present experimental system. This kind of behavior has already been reported in literature for functionalized PMMA/PHSA particles dispersed in dodecane and corresponds to a charge regulation mechanism (see ⁴ and references therein). Interestingly, the range of electrostatic interactions is measured to be of the order of 10 μ m in the present system, which corresponds to 10 particle diameters. This explains why the particle collective diffusion coefficient is very large compared to the Stokes-Einstein value even in what would seem dilute conditions (volume fraction less than 0.26%).

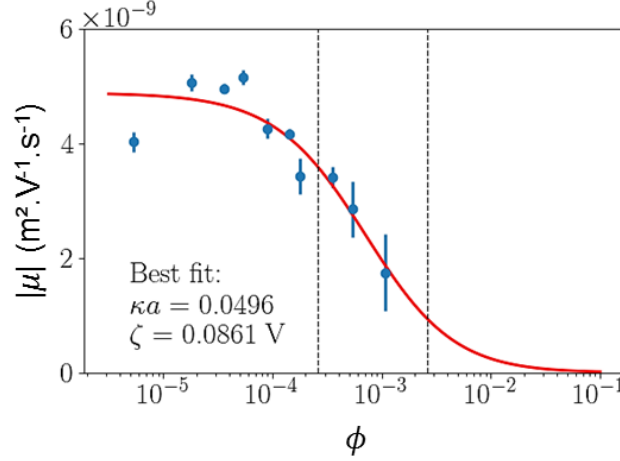


Figure S4. Electrophoretic mobility variation as a function of the volume fraction for 1 μ m latex particles. Experimental data: blue symbols; Model: red curve. The vertical dashed lines indicate the range of volume fractions corresponding to the range of bulk particle concentrations C_b investigated in the article ($C_0/5 < C_b < 2C_0$).

Particle-substrate electrostatic force modelling

A model for the particle-substrate electrostatic force is required to solve the transport equation in the first regime. This regime corresponds to the capture of particles above the substrate at a distance smaller than about one or two Debye lengths. Unfortunately, classical DLVO-type force models are in principle valid for separation distances larger than that. To determine which model can be used in the transport equation, we performed full 3D Debye-Hückel simulations of one particle above a charged plate and measured the interaction force for the physico-chemical conditions used in the many-body simulations. The results are reported in **Fig. S5** as a function of the separation distance y scaled by the Debye length. The linear superposition approximation (LSA)⁴

$$F_{LSA} = -\epsilon \left(\frac{kT}{e} \right)^2 4\pi\kappa a \psi_s \psi_p e^{-\kappa(y-a)} \quad (3)$$

underestimates the interaction force for all the distances investigated. This was expected as this is a result derived in the limit of weakly overlapping double layers. The Hogg, Healy & Fuerstenau (HHF) approximation⁵

$$F_{HHF} = -\epsilon \left(\frac{kT}{e} \right)^2 2\pi \kappa a \frac{2\psi_s \psi_p e^{-\kappa(y-a)} - (\psi_s^2 + \psi_p^2) e^{-2\kappa(y-a)}}{1 - e^{-2\kappa(y-a)}} \quad (4)$$

is in better agreement with simulations. It recovers numerical results perfectly as soon as $\kappa y > 1$. Solving the transport equation with this full equation is however difficult. In order to have a tractable equation, we used the force model $F = \alpha F_{LSA}$ shown in red in **Figure S5**. The LSA force form (which is the same as the large distance HHF force) makes the transport equation tractable, but it has to be modified with the factor $\alpha = 1.6$ here to have a reasonable agreement with the simulations for the distances $\kappa y < 2$ of interest in the first capture phase.

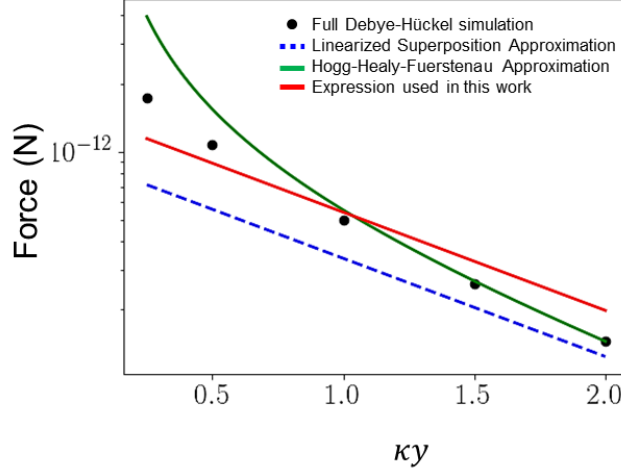


Figure S5. Particle-substrate electrostatic force as a function of distance for an isolated particle. The parameters are those used in the article. Black symbols: full Debye-Hückel simulation of one particle and a charged wall; Green curve: Derjaguin approximation (1); Blue dashed line: Linearized Superposition Approximation (2); Red line: expression used in this article (3).

Collective diffusion coefficient calculations

The value of the collective diffusion coefficient can be calculated with the generalized Stokes-Einstein relation $D = D_0 f / \chi$ where f is the sedimentation hindrance function and χ is the osmotic compressibility. For the hydrodynamically dilute dispersions considered here $f \approx 1$. As the mean surface to surface distance between particles in the bulk is at most $l_{s-s} \approx d \left(\phi^{-\frac{1}{3}} - 1 \right) = 1.7l_D$ in the simulations presented here, with ϕ the volume fraction, electric double layers interact everywhere and the osmotic compressibility can be calculated accurately with the cell model^{6,7}. For the system considered in **Figure 2b**, we obtain $D \in [220D_0, 245D_0]$.

Influence of the particle concentration

Figure S6 shows the $1\mu\text{m}$ normalized pattern and background particle densities of assemblies made by convective nanoxerography at different concentrations from $\rho_0/5$ to $2\rho_0$ where $\rho_0=6.825\times 10^8\text{ mL}^{-1}$. The static contact time was set to 0, with a dragging speed at $8\mu\text{m}\cdot\text{s}^{-1}$ leading to $t_{tc} = 275\text{s}$.

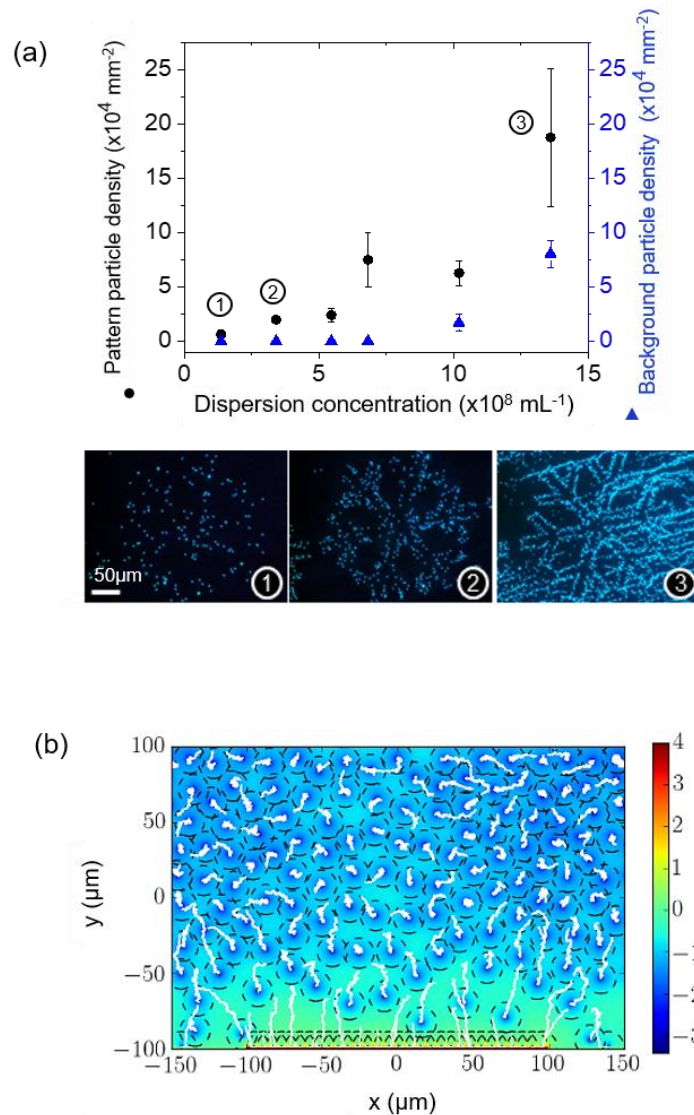


Figure S6. (a) Pattern and background particle densities as a function of the dispersion concentration for $1\mu\text{m}$ latex particles with fluorescent optical microscopy images of numbered assemblies, (b) Numerical simulations of particles trajectories above the charged pattern. The electrostatic potential field is the one obtained for the final simulation time. The bulk particle density is $\rho_b = 1.37 \times 10^9\text{ mL}^{-1}$

Both densities are increasing with the dispersion concentration, a conclusion that has also been reported in the case of smaller particles assembled by nanoxerography.⁸ Indeed, by extending the number of particles in the dispersion drop, the probability to locate some of them close

enough to the charged pattern to induce electrostatic attraction and the convective flux density ρu are both increased linearly. The numerical simulation configuration with a high number of particles presented on **Figure S6b** shows that particle screening lengths are recovering from one particle to another at such concentration which makes the effective diffusion coefficient D increase by coulombic repulsions. The negatively charged particles quickly deposited onto the charged pattern, by electrostatic attraction in the area $y < l_D$, do not screen the electric potential generated by the positive patterns which allows the deposition of additional particles and the pattern particle density increase by carrying on the development.

Finally, a working concentration of $\rho_b = 6.825 \times 10^8$ Ps/mL gives a pattern particle density high enough with a good selectivity.

Influence of the substrate temperature

An analysis of the influence of the substrate temperature on $1\mu\text{m}$ particles assemblies has also been done. Results are shown in **Figure S7**.

Pattern and background particle densities increase with the substrate temperature from a threshold $T_{\text{th}} = 20^\circ\text{C}$. By using real-time optical microscopy recordings, one can see that the convective flow rate speeds up for temperatures higher than T_{th} . The solvent evaporation rate increases with the temperature difference between the top of the drop, corresponding to the room temperature, and the edge of the drop,⁹ the temperature of the heated substrate. For the range of temperatures investigated (17 to 25°C), the vapor pressure increases roughly by a factor two. Consequently, the solvent evaporation rate directly increases with the substrate temperature and makes the convective flow speed up, which increases the particle flux towards the triple line. In addition, the viscosity of the solvent heated by the substrate diminishes by about 30%, and the particle diffusion coefficient D_0 increases by about 30%. Both phenomena facilitate particle displacements to the edge of the meniscus. A working temperature just below T_{th} prevents the predominance of convective flow effects and allows the analysis of other parameters.

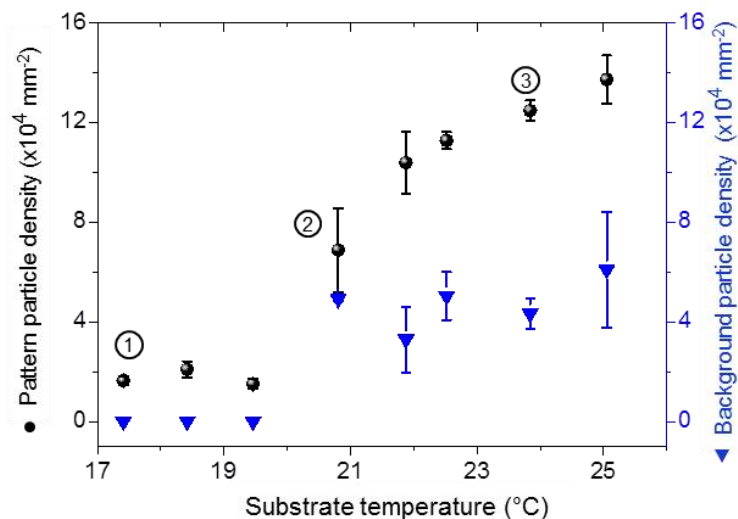


Figure S7. 1 μm latex particle pattern and background densities as a function of the stage temperature and fluorescent optical microscopy images of numbered assemblies.

Initial contact time influence on the convective flow assembly of 500nm and 4.3 μm

The initial contact time influence on the assembly of 500 nm and 4.3 μm latex particles assembled by a convective flow development method was analyzed as for the 1 μm particles. **Figures S8 and S9** present the corresponding results.

The experimental curve for the 500 nm particles was fitted with a function $f(t) = At^b$, where $A = 3220 \pm 179 \text{ Ps. mm}^{-2}$ and $b = 0.40 \pm 0.01$. The shape of the fitting curve is close to a $\sim \sqrt{t}$ function pointing out a diffusion mechanism.

Fitting correctly a $\sim \sqrt{t}$ function was not possible for the 4.3 μm particles. It might be because of the sedimentation phenomenon involved in their assembly. Indeed, their sedimentation speed is about 18 times higher than that of 1 μm particles. In addition, 4.3 μm particles are more likely to roll on the substrate surface to move towards or away from charged patterns due to electrostatic or hydrodynamic forces.

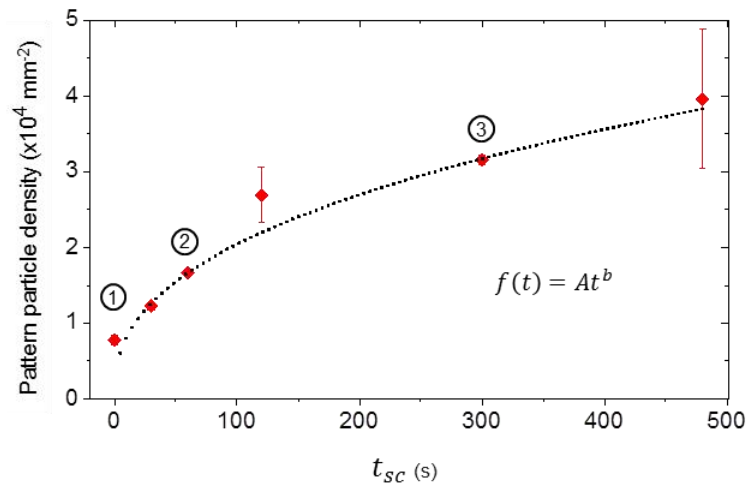


Figure S8. Pattern particle density as a function of the static contact time t_{sc} before the 500 nm latex dispersion drop dragging and fluorescent optical microscopy images of numbered assemblies.

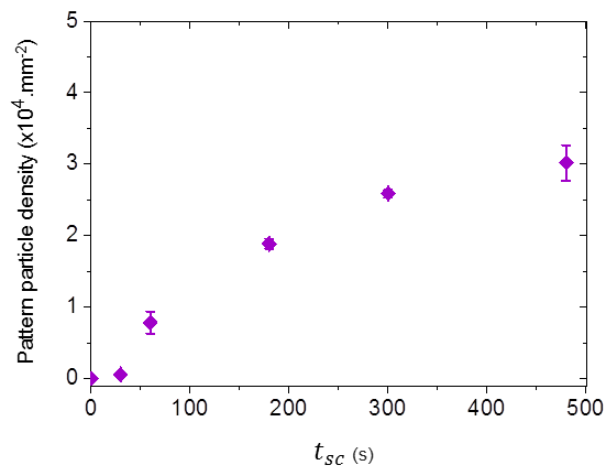


Figure S9. Pattern particle density as a function of the static contact time t_{sc} with a dragging speed of $80 \mu\text{m}\cdot\text{s}^{-1}$ for $4.3 \mu\text{m}$ latex particles

REFERENCES

- (1) Teulon, L.; Palleau, E.; Morales, D.; Poirot, D.; Ressier, L. Interactive Nanogel Marking at the Microscale for Security and Traceability Applications. *Adv. Mater. Technol.* **2018**, *3*, 1700244.
- (2) Cau, J.-C.; Ludovic, L.; Marie, N.; Adriana, L.; Vincent, P. Magnetic Field Assisted Microcontact Printing: A New Concept of Fully Automated and Calibrated Process. *Microelectron. Eng.* **2013**, *110*, 207–214.
- (3) Ohshima, H. Electrophoretic Mobility of Spherical Colloidal Particles in Concentrated Suspensions. *J. Colloid Interface Sci.* **1997**, *188*, 481–485.
- (4) Bell, G. M.; Levine, S.; McCartney, L. N. Approximate Methods of Determining the Double-Layer Free Energy of Interaction between Two Charged Colloidal Spheres. *J. Colloid Interface Sci.* **1970**, *33*, 335–359.
- (5) Hogg, R.; Healy, T. W.; Fuerstenau, D. W. Mutual Coagulation of Colloidal Dispersions. *Trans. Faraday Soc.* **1966**, *62*, 1638–1651.
- (6) Hallez, Y.; Diatta, J.; Meireles, M. Quantitative Assessment of the Accuracy of the Poisson–Boltzmann Cell Model for Salty Suspensions. *Langmuir* **2014**, *30*, 6721–6729.
- (7) Deserno, M.; Holm, C. Cell Model and Poisson-Boltzmann Theory: A Brief Introduction. *ArXivcond-Mat0112096* **2001**.
- (8) Sangeetha, N. M.; Moutet, P.; Lagarde, D.; Sallen, G.; Urbaszek, B.; Marie, X.; Viau, G.; Ressier, L. 3D Assembly of Upconverting NaYF₄ Nanocrystals by AFM Nanoxerography: Creation of Anti-Counterfeiting Microtags. *Nanoscale* **2013**, *5*, 9587.
- (9) Bhardwaj, R.; Longtin, J. P.; Attinger, D. Interfacial Temperature Measurements, High-Speed Visualization and Finite-Element Simulations of Droplet Impact and Evaporation on a Solid Surface. *Int. J. Heat Mass Transf.* **2010**, *53*, 3733–3744.